PFC/JA-86-31

Improved Plasma Startup in the Tara Central Cell

R.S. Post, K. Brau, S. Golovato, E. Sevillano,
D.K. Smith, W. Guss, J. Irby, R. Myer, J. Sullivan

May 1986

Plasma Fusion Center
Massachusetts Institute of Technology
Cambridge, Massachusetts 02139 USA

Submitted for publication in Nuclear Fusion.

Improved Plasma Startup in the Tara Central Cell

R. S. Post, K. Brau, S. Golovato, E. Sevillano, D. K. Smith
W. Guss, J. Irby, R. Myer, J. Sullivan

ABSTRACT

A new gas fueling and magnetic field configuration of the central cell of the Tara Tandem Mirror is described which achieves parameters necessary to establish and maintain both a sloshing ion population and thermal barriers in the axicells. Gas injection at the central cell midplane leads to low neutral pressures in the axicell and minimizes losses of sloshing ions due to charge exchange with background gas. A magnetic maximum at the Tara midplane divides the central cell into two R=2 mirrors in order to isolate the region of hot ions trapped magnetically in the local mirrors from the gas injection location at the magnetic maximum, and thereby reduce the effect of charge exchange recombination on the energy confinement time. The midplane magnetic "bump" also permits launching of a slow wave by an ICRF antenna located near the midplane that is efficiently absorbed at the resonances near the bottom of the magnetic wells on either side. Numerical simulations based on current central cell parameters and response time of the gas fueling indicate that the central cell density rise at thermal barrier onset can be controlled, thereby preventing collisional filling of the thermal barrier by the central cell ion stream.

Introduction

Most tandem mirrors rely on a combination of neutral beam injection and electron cyclotron resonance heating (ECRH) in the end (plug) cells in order to create the positive electrostatic potentials which confine the central cell ions. The success of this scheme depends upon establishing a target plasma in the end cells of sufficient density and temperature to permit sloshing ion buildup by high energy neutral beam injection and thermal barrier formation by ECRH. Three schemes have been used to produce the target plasma: (1) gun injection from the end wall, (2) gas puffing in the central cell and ECRH in the end plug, and (3) central cell startup by ion cyclotron resonance heating (ICRH). Gun injection is not desirable since it produces high plasma density near the end walls, leading to high thermal conduction losses, and it may also be a source of impurities. Injecting gas directly into the central cell with ECRH in the plug does not result in direct ion heating. The temperature of the plasma which streams from the central cell into the plug is limited, leading to high collisional filling rates in the thermal barrier. Producing a plasma first in the central cell and using the ICRF heated loss stream through the end plug as a startup target can circumvent these problems.

In the Tara tandem mirror the central cell startup plasma is generated by purely RF means. A similar technique was first proposed by Post, et al.[1,2] and later performed on the Phaedrus tandem mirror.[3] In Tara, a plasma stream produced by ECRH in the minimum-B MHD anchor cells produces a low density preionization plasma in the central cell. Gas puffing and ICRH in the central cell build up the plasma to sufficiently high density and temperature to provide an adequate stream in the end plug for a startup target. Different combinations of gas injection, magnetic field profile, and ICRH have been explored in order to minimize neutral gas levels in the end plugs and to produce sufficiently high ion end loss temperatures to reduce collisional filling of the thermal barrier to an acceptable level.

The purpose of this paper is to characterize the central cell plasma obtained using two of these configurations, and in particular, to emphasize the advantages of the most recent one, which involves midplane fueling into a region of locally high magnetic field. All of the data discussed below were obtained without neutral beam injection in the plugs. Preliminary experiments with neutral beam injection and ECH in the plugs have not yet

led to unambiguous thermal barrier formation; however, it appears that the problems with obtaining full tandem mirror operation are related to issues of stability, and not to the central cell stream, which has proved to be adequate.

This paper is organized as follows. In section II we describe the different gas fueling configurations that have been studied, and touch upon the problems with the earlier versions which motivated the latest configuration. A description of central cell antennas and the physics of ICRF heating will follow. Section III is a summary of experimental results obtained with two of the startup configurations, focussing on a comparison of stream parameters in the plug, and on fueling efficiency, energy and particle confinement in the central cell.

Gas fueling configurations

The Tara tandem mirror is a composed of a 10 meter long central cell bounded on each side by an axisymmetric plug cell and an outboard minimum-B MHD anchor cell. Both the thermal barriers and potential barriers are created in the plugs. Hence most ions will see only an axisymmetric magnetic field, which reduces classical radial ion diffusion due to nonaxisymmetric fields (neoclassical transport). The central cell plasma is heated by three ICRH antennas. Results presented in this paper were obtained without neutral beams or ECRH in the plugs.

Critical to central cell plasma startup is the choice of gas fueling location. Three different gas injection configurations have been tested in the Tara central cell. In the first, represented schematically in fig. 1a, gas was injected near the R=1 point where the ion cyclotron resonance was located. Gas pressures were correspondingly high in the heating region, and charge exchange recombination between the hot mirror confined ion component and neutral hydrogen was found to reduce severely the ion energy confinement time.

To isolate the region of high neutral pressure from the mirror confined ions, the gas injection locations were moved to the high mirror ratio (R=4) points at the ends of the central cell, as is indicated on the same figure. Gas was injected into two "gas boxes" at the R=4 positions, which were designed to confine the high neutral pressure region to a small volume (less than 10 cm axially). Typical injection rates for these discharges were

on the order of 5-15 torr-liter/sec on each side.

An axial profile of the neutral gas measured by a series of fast ion gauges for a standard ICRF heated discharge is indicated by the solid curve in fig. 2. Approximately 350 kW of power was forward coupled by two antennas. At the gas injection points the neutral pressure is in the millitorr range, dropping to the low 10^{-6} torr range at the midplane. (The north-south pressure profile asymmetry was due to a leak in the south gas box.) The neutral pressure in the south plug is 3×10^{-6} torr. This is roughly an order of magnitude higher than the level at which charge exchange recombination of high energy beam ions with neutral hydrogen is predicted to suppress sloshing ion buildup. Despite the use of limiters at the ends of the central cell (between the gas box and the plug) it is clear that much of the gas goes directly into the end plug.

An equally serious drawback to this gas injection configuration is that it produces a cold ion stream to the plug. The potential at the central cell midplane is higher than the R=4 gas injection point for two reasons. Since the ICRF heated ions are mirror confined, the density at the central cell midplane (R=1) is higher than at R=4, causing a minimum potential rise of $\Delta\Phi = T_e \ln[n_c(R=1)/n_c(R=4)]$. Secondly, the ICRF produces a non-Boltzmann potential through directed interaction with electrons.[4,5] The effect of this potential was clearly demonstrated by measurements of the ion endloss with fueling on only one side of the central cell.[6] The endloss ion currents from the fueled end are a factor of three to five higher than the unfueled end. Hence a significant fraction of the ionization source is never heated as it cannot reach the resonance zone. This plasma flows into the thermal barrier unheated and traps there, defeating the thermal isolation.

These problems motivated a redesign of the gas fueling indicated schematically in fig. 1b, Gas is injected near the central cell midplane to prevent leakage into the plugs. To avoid the problem of high neutral pressure near the ICRF resonance the magnetic field is increased in an approximately two meter section about the midplane dividing the central cell into two R=2 mirror regions. This permits the ICRF antenna located near the midplane magnetic maximum to excite a slow ion cyclotron wave which is efficiently absorbed at resonances near the magnetic minima on either side of the midplane. The remaining two antennas (see next section) are also operated at frequencies so that ions

are resonant near the bottom of the magnetic well. Ions created in the ionization volume near the midplane must pass through a resonance at least once before continuing on to the plug. RF trapping of the cold ions from the fueling region[7] increases $T^{cc}_{\|,i}$ and reduces the collisional thermal barrier filling rate.

Some of these ideas are illustrated in the velocity space diagram for the axicell midplane, shown in fig. 3. The trapping region for central cell ions is indicated by the solid lines, which intercept the $v_\|$ axis at points corresponding to the thermal barrier electrostatic well depth. The dotted lines which intercept this axis at larger values of $v_\|$ indicate the combined electrostatic and magnetic trapping of plug ions due to the difference between the central cell and plug potentials. For the case of R=4 fueling ions are born in the small dark quarter circular regions adjoining the trapped boundary. These low energy ions have a high probability of diffusing into the trapped region by collisions with the background ions. With midplane fueling, indicated schematically by the shaded quarter circular regions, the average energy of the ions entering from the central cell is higher, and thus the velocity space gradient across the trapped boundary and the collisional diffusion into the thermal barrier are reduced.

As long as the region of high neutral pressure remains localized to the midplane, the particle confinement time of ions deeply trapped in the R=2 mirrors is expected to approach the pitch angle scattering time to the midplane. During startup the gas box pressure is such that an ion scattering into the midplane has a high probability of being lost by charge exchange. The midplane gas box, shown in cutaway view in fig. 4, is designed to confine the high pressure region to a small well-defined volume. Gas is injected at two azimuthal positions 180° apart into a 53 cm long, 40 cm diam. cylinder with annular baffles. The purpose of the baffles is to prevent neutral hydrogen molecules from flowing axially without first passing through the ionization region. Two diffusers were added at the injection points to produce more azimuthally uniform fueling. Additional baffling is provided by a set of limiters between the gas box and the magnetic well designed to separate the high neutral pressure region from the hot magnetically trapped ion region. Bounding the gas box are two electrically floating eight-segment limiters which measure an azimuthal distribution of the edge plasma current. These two limiters define the plasma radius throughout the

machine.

The dashed curve in fig. 2 is a plot of the axial profile of the edge neutral pressure measured by fast ion gauges during a typical midplane fueling discharge. The neutral pressure drops by a factor of twenty between the injection point and a position 50 cm away, indicating that the high pressure region is well localized. The edge neutral pressure at the magnetic wells scales with the plasma pressure and thus is due primarily to recycling at the walls caused by ion bombardment. Most importantly the neutral pressure in the plug has been reduced by an order of magnitude compared with the R=4 fueling case, and is now at acceptable levels.

The gas box and the injection scheme are described in more detail elsewhere.[8] Control of the injection rate is based on pulse width modulation of piezoelectric valves. The injection rate can be varied during a shot by changing the duty cycle of a square wave applied to the piezoelectric valves. An interesting phenomenon is observed if only one of the two piezoelectric valves is used during a discharge. The line integrated H_α emission exhibits a 25% modulation in amplitude at the piezoelectric valve modulation frequency. This indicates a strong coupling of the light emission to the gas injection rate. In general signals which depend the most on the neutral density (e.g. H_α emission, secondary emission detectors, antenna reflection coefficient) appear to be the most sensitive to the modulation rate. This coherent modulation can be avoided by using two piezoelectric valves and a gas ballast tank. It does indicate, however, that the response time of the gas box is at least as short as 1 msec and that the volume in which ionization occurs is well contained within the gas box. A short response time is needed because at the onset of thermal barrier formation the central cell axial confinement time will improve by an order of magnitude, leading to a rapid rise in central cell density. This density rise may lead to a catastrophic increase in the collisional filling rate of the thermal barrier. We have attempted to model the time evolution of the filling rate following thermal barrier onset, assuming constant central cell energy particle confinement time and RF power, and different values of the initial filling rate and of the pumping rate by neutral beam injection. In each case the density of cold trapped ions in the thermal barrier initially decreases, then as the central cell density rises beyond a certain level, a very rapid (order of 100 microseconds) increase of the trapped

ion fraction in the thermal barrier occurs, effectively destroying it. Hence, to prevent the central cell density rise, the injection rate must be reduced very rapidly at thermal barrier onset.

ICRF Antenna Operation

Three antennas are used for ICRF experiments in the central cell—two "double half-turn" loop antennas and one "slot" antenna. Each double half-turn antenna consists of a continuous 23.5 cm radius circular loop of 10 cm wide copper strap fed at the top and bottom so that current flows through the two halves in parallel (fig. 5). The loop antennas are protected from direct plasma contact by limiters separated by 10 cm axially from the antenna edges. Each antenna is bounded by two of these limiters extending from the vacuum wall inward to a radius of 22.5 cm. The loop antennas have an inductance of about 400 nH, a quality factor of greater than 100, and typically operate with a radiation resistance due to plasma loading of 0.3Ω. Operation at 200 kW per antenna then results in 10 kV on the vacuum feedthrough insulator.

The slot antenna is a copper cylinder 20 cm in radius and 80 cm long. The essential parts of the antenna are a pair of apertures (slots) 40 cm long by 15 cm high on opposite sides of the plasma (see fig. 5). Current flow is localized to the circumference of the apertures and flows so as to produce a relatively uniform radial magnetic field over each aperture. This field and current distribution has been confirmed by bench testing of the antenna. The direction of the radial magnetic field is inward on one side and outward on the other defining a linearly polarized RF magnetic flux bundle transverse to the axis of the plasma. Based on bench measurements of the antenna fields a model of the antenna as an infinite conducting cylinder with a uniform radial magnetic field incident over the apertures was developed and included in the ANTENA code.[9] The ANTENA code with this model is used to calculate the wave fields of the antenna in the presence of the plasma column.

The current paths and resulting fields and plasma coupling are similar to those of the Nagoya Type III antenna.[10] A unique feature of the slot antenna compared to the Type III or loop antennas is that essentially all of the magnetic flux produced by the

antenna passes through the plasma column. The other types of antennas generally have large amounts of private flux which do not link the plasma and therefore add unnecessarily to the antenna voltage. The low inductance 350 nH and typically high (R > .5Ω) plasma radiation resistance of the slot allow 600 kW operation with only 6 kV on the feedthrough insulators.

The excitation properties of the slot and double-half-turn antennas differ in two ways that are important for the Tara start-up configuration. First, the slot antenna produces a z-directed RF electric field, E_z, in vacuum due to z-directed current flow in the antenna. It can therefore couple power to electrons by Landau damping in vacuum or very low density plasma. The double-half-turn antenna produces no vacuum E_z and plasma space charge is required for E_z to be generated. Second, the axially-spaced, oppositely directed currents on either side of the apertures of the slot antenna excite a spectrum which peaks at larger axial wave number, k_z, than the double half-turn antenna. This is shown in fig. 6 where the calculated vacuum k_z spectra of the left circularly polarized electric field, E_+, for the two antennas are plotted for azimuthal mode number $m = -1$. The slot antenna more readily excites lower phase velocity waves. Two axially spaced, oppositely phased double half turn antennas would be necessary to accomplish the same results.

By placing the gas box and slot antenna on a bump in the magnetic field at the central cell midplane, the two important features of the slot antenna just discussed, i.e. large E_z and k_z may be exploited. The proximity of the slot to the gas box allows the vacuum near-fields at the antenna, in particular E_z , to break down the fueling gas more easily and build up the plasma. The RFC-XX experiment also feeds gas close to their Type-III antenna for this reason.[11] Typically, for midplane fueling, gas is injected 7-9 msec before the slot antenna is excited in order to have sufficient gas for plasma buildup. For R = 4 fueling, gas had to be injected 20-30 msec in advance of slot excitation to have sufficient gas in the vicinity of the antenna near-fields, which were 4 meters from the R = 4 gas box. Another indication of the importance of the vacuum E_z field is the inability to achieve startup using only the double- half-turn antennas in either fueling configuration. Half-turn loops have been used to buildup and sustain plasma in the Phaedrus Tandem Mirror with direct ECRH in the central cell to produce densities above 10^{11}cm^{-3}. In this way, the

half-turn antenna could excite an E_z field to couple to the electrons. Buildup could not be achieved on Phaedrus with lower ECRH-produced initial densities.[12] In Tara only a weak plasma stream from a 14GHz ECRH plasma produced in an anchor cell 10 m from the central cell midplane is necessary to create a central cell plasma with the slot antenna. Prior to slot operation the density in the central cell is less than $4 \times 10^{10}\text{cm}^{-3}$. Even this small initial plasma density is necessary for plasma buildup with the slot antenna. If only gas and ICRH is used, breakdown will occur first at high voltage gaps in the antenna feeds rather than in the confined flux tube of the tandem mirror.

The midplane magnetic bump allows the slot antenna to excite slow, ion cyclotron waves. These modes should be readily excited at $\omega < \omega_{ci}$ using the natural wave spectrum of the slot antenna and propagate down the gradient to an ion cyclotron resonance near the magnetic field minimum. For the conditions in the Tara central cell, only the $m = 1$ fast wave can propagate and it produces primarily a right-circularly-polarized electric field, E_-, in the plasma core and E_- does not couple to ions.[13] Figure 7 shows the dependence of the plasma diamagnetism on position of the resonance with respect to the magnetic well. These data were taken by varying the minimum field in the central cell with the midplane field and RF frequency held fixed. There is an optimal resonance for good heating, with best results for the resonance at a mirror ratio of 1.1. The sharp fall-off in diamagnetic signal at higher fields is due to reduced heating efficiency while at lower field it is due to an MHD instability.[14]

That the best heating occurs with the resonance a meter from the antenna is indicative of heating by a propagating mode, not near-fields. Under optimum conditions RF is excited with $\omega/\omega_{ci} = 0.6$ at the midplane. At this value of ω/ω_{ci} the slot antenna spectrum is well matched to the slow wave dispersion relation. The cold plasma dispersion relation for the slow wave yields two real values of $k_\perp$ (wave number perpendicular to the magnetic field) for each k_z. At $\omega/\omega_{ci} = 0.6$ the slot antenna can couple to slow modes with both $k_\perp$ real, while $k_\perp$ is imaginary for the fast wave, (except $m = 1$ as mentioned previously). Therefore the slow wave fields propagate into the plasma and produce better heating of the core plasma ions. At higher values of ω/ω_{ci}, where the slow wave k_z increases, the slot antenna would couple to it more poorly. Both the double-half-turn antenna and

the slot antenna heat best with predominantly near-field heating at $\omega/\omega_{ci} \simeq 1$ when positioned at the minimum magnetic field, since the fast wave modes with appreciable E_+ are nonpropagating. Improved core coupling by the slow wave is shown by profiles of the ion endloss. Figure 8 shows signals from an array of Faraday cups on the end wall which collect ion current. With slot antenna heating, a more peaked profile is seen compared to the broader, flat profile for near-field heating with either the double-half-turn antennas or slot heating without the midplane bump. It should be mentioned that a double-half-turn antenna could also couple to slow waves if positioned on the midplane bump, but its k-spectrum is less well suited than the slot.

Experimental Results

In a previous section the advantage of the midplane fueling compared with R=4 fueling was demonstrated in regard to the neutral pressure in the plugs. In this section we will discuss the improvements in core power coupling of the slot antenna that resulted from the new configuration. We shall first characterize the central cell plasmas obtained with both configurations, and then compare the respective plug stream parameters.

Three cases will be considered: 1) R=4 fueling with slot antenna heating only, 2) R=4 fueling with primarily double half-turn antenna heating, and 3) midplane fueling with slot antenna heating only. Figure 9a shows plots of the time history of the ICRF power, diamagnetic loop signal at R=1, expressed as percent $\beta_\perp$, line integrated density, and global central cell energy confinement time τ_E^g, defined as the ratio of volume averaged plasma energy content deduced from diamagnetic loop measurements to total RF input power, for the case of R=4 fueling with slot antenna only. The values of the density and plasma beta are obtained assuming flat density and temperature profiles out to the limiter radius of 15 cm. The global energy confinement time is about 40 μsec. A second measurement of the energy confinement time, τ_E^d, is obtained from the decay of the diamagnetism after the end of the RF pulse. In general this decay can be modelled by a double exponential curve, with the first time scale corresponding to the initial rapid decrease and the second time scale to the slower decay at the end. We equate τ_E^d with the first time scale. For these data $\tau_E^d = 250\mu$sec. In the event that all of the RF power is coupled to the core ions, τ_E^g

should equal τ_E^d. Their ratio, then, is a measure of the coupling efficiency of ICRF power to the core ions, which is about 16% for this discharge.

In fig. 9b, also R=4 fueling, the slot antenna was used only for plasma buildup, then turned off after 10 msec with the double half-turn antenna sustaining the plasma. From the diamagnetic loop signal we obtain $T_{i\perp} + T_e \simeq 100$ eV at t = 10 msec. The electron temperature measured independently by Langmuir probes was 30 eV. For this discharge $\tau_E^g \simeq 100 - 120\mu$sec, and $\tau_E^d \simeq 350\mu$sec, giving a core ion coupling efficiency of 0.3, which is almost twice that for the slot antenna alone in a uniform field.

In fig. 10 data are plotted from a midplane fueling discharge with slot antenna only. In steady state $T_{i\perp} + T_e = 300$ eV, $\tau_E^g \simeq 120\mu$sec, and $\tau_E^d \simeq 480\mu$sec. This gives a core ion coupling efficiency of 0.25, which is somewhat less than that obtained with R=4 fueling and double half-turn antenna only. The plasma $T_{i\perp} + T_e$ is higher because of greater RF power input.

The τ_E^g and τ_E^d are somewhat improved in the midplane fueling configuration. For the ion temperatures obtained so far the pitch angle scattering time into the region of high neutral gas pressure is short compared with the charge exchange time at the magnetic minima. The ion energy confinement is therefore a combination of pitch angle scattering into the gas box region and charge exchange. In fig. 11 the central cell τ_E^g is plotted against neutral pressure at the gas injection point. The inverse scaling of τ_E^g with gas box pressure confirms that energy confinement is dominated by charge exchange. To reduce the role of charge exchange requires lowering the neutral pressure in the gas box. At the onset of thermal barrier formation the central cell gas injection rate will need to be reduced by at least an order of magnitude. Theoretically the central cell energy confinement time will then equal the pitch angle scattering time of ions in the R=11 mirrors.

Another indication of the comparative quality of the two configurations is the gas utilization efficiency. Because of the transparency of the central cell plasma to Franck-Condon hydrogen atoms, the charge exchange recombination rate with current parameters can be minimized only by a reduction in the gas fueling rate. The gas utilization efficiency is defined as the ratio of electron end loss current to gas injection rate (both measured in amps). In the limit of purely axial electron loss (no ambipolar transport) and no neutral

gas recycling, this ratio is a measure of the fraction of injected gas which is ionized. The electron endloss current is determined by subtracting the area integrated signals from the Faraday cup array from the signals of the net current detectors. Figure 12 is a plot of electron endloss current vs. gas injection rate for the R=4 and midplane fueling cases. Although a consistent data set at various injection rates was not obtained for the R=4 configuration, clearly the gas utilization efficiency is about a factor of two lower than the comparable midplane fueling value. For midplane fueling the efficiency is approximately constant for injection rates less than 100 amp neutral equivalent, then decreases with increasing fueling rate. Numerical modeling of the neutral density profile with a 1-D Monte Carlo simulation indicates that the improved efficiency of the midplane fueling configuration is due almost entirely to a larger ionization volume at the injection points.

The primary motivation behind the reconfiguration of the central cell gas injection system and magnetic field was to provide a dense stream to the plug to act as a target for neutral beam buildup, and one that is sufficiently hot to prevent collisional filling of the thermal barrier. The plug neutral density is measured by microwave interferometers and the ion stream temperature by a set of gridded electrostatic analyzers located at the end walls.

We may demonstrate the importance of gas control and stream temperature to the maintenance of a thermal barrier by a numerical simulation. In this model the total RF input power to the central cell ions is assumed constant. Therefore,

$$P_{rf} = \frac{3}{2}\frac{n_e k T_i}{\tau_E} = const \tag{1}$$

implies

$$\frac{1}{n_e}\frac{dn_e}{dt} - \frac{1}{T_i}\frac{dT_i}{dt} - \frac{1}{\tau_E}\frac{d\tau_E}{dt} = 0 \tag{2}$$

The equation for the central cell density is given by

$$\frac{1}{n_e}\frac{dn_e}{dt} = \frac{1}{\tau_{ion}} - \frac{1}{\tau_p} \tag{3}$$

where $\tau_{ion} = 1/n_0\langle\sigma v\rangle_{ion}$ is the ionization time and τ_p is the total particle confinement time.

The trapped density in the barrier n_t is given by

$$\frac{1}{n_t}\frac{dn_t}{dt} = \nu_{FL} - \nu_{pump} + \nu_{ion} \tag{4}$$

where ν_{FL} is the Futch-LoDestro [15] barrier trapping rate, ν_{pump} is the pumping rate from the neutral beams and ν_{ion} is the filling rate of the barrier due to ionization processes of the background gas. The pumping rate is estimated using 75 A of 20 kV neutral beams on target and a beam footprint of 200 cm^2, which gives $\nu_{pump} = 3100$ sec^{-1}. The ionization term, which is estimated using a background neutral pressure in the barrier of 5×10^{-7} Torr and assuming no neutral gas attenuation, is $\nu_{ion} = 500$ sec^{-1}. These terms are assumed constant in the model. The Futch-LoDestro term is given by

$$\nu_{FL} = \frac{n_p}{n\tau_{ii}}[0.94(1+0.0441R_b)]^{3.3}\left(\frac{g}{g-1}\right)^{3.3} \tag{5}$$

where n_p is the passing density, $n\tau_{ii} = 1.4\times10^7 T_i(\mathrm{eV})^{3/2}/ln\Lambda$ cm^{-3}sec for hydrogen, $g = (n_p + n_t)/n_p$ and $R_b = 5$ is the mirror ratio of the axicell. For large R_b the passing density is related to the central cell density by

$$n_p = \frac{n_c}{R_b}\frac{1}{(\pi\phi_b/T_i)^{1/2}} \tag{6}$$

We follow the time evolution of the trapped barrier density given by Eq. (4) using Eqs.(2), (3), (5) and (6) keeping $\phi_b/T_i = 2$. Thermal barrier filling is most sensitive to the ion stream temperature T_i and the passing density, which in turn is related to the central cell density n_c by Eq. (6). In the model we specify the initial central cell density, initial ion temperature, the characteristic decay time of the neutral gas τ_{gas} (related to the response time of the gas box described earlier) and the particle confinement time prior to plugging. At the onset of plugging the particle confinement improves significantly and therefore the central cell density increases exponentially with a characteristic time constant given by the particle confinement time prior to plugging. Since by assumption the RF power remains constant, the ion temperature would decrease unless the energy confinement time of the ions improved. Because this energy confinement is charge exchange dominated, endloss plugging may not change it significantly, however; a reduction of the neutral gas would

improve it. Since as the neutral gas is reduced other ion energy loss channels would become important, we limit the temperature increase to twice its initial value.

In fig. 13 the trapped density, central cell density, ion temperature, and the quantities g and ϕ_b/T_e are plotted vs. time for three different cases of T_i and response time of the gas box. All the values are normalized at $t = 0$. For the base case shown in fig. 13a we choose typical Tara startup parameters $T_i = 60$ eV and $n_e = 2.5 \times 10^{12}$ cm^{-3}. The response time of the gas injection system is taken to be 3 ms. The increase of the trapped density can be controlled in this case indicating that a thermal barrier can be maintained. Figure 13b shows the results if the response time of the gas fueling is increased to 6 ms. In this case the fueling is not reduced quickly enough to prevent the central cell density from rising too rapidly, and the barrier fills quickly as indicated by the rapid rise of the trapped density. Finally, fig. 13c shows the effect of reducing the parallel ion stream temperature to $T_i = 35$ eV, which was typical of fueling at the $R = 4$ mirror ratio. The barrier is again lost by collisional filling.

Summary

We have described a new configuration of gas injection and ICRF heating in the Tara central cell designed to produce an adequate stream to the plug cells permitting sloshing ion buildup and thermal barrier formation. This configuration satisfies the following three essential criteria: low neutral pressure in the plug to prevent charge exchange losses of sloshing ions, sufficient plasma density to provide an adequate beam target, and high parallel ion temperature to prevent collisional filling of the thermal barrier. By creating a local maximum in the magnetic field at the central cell midplane, the slot antenna can launch a slow ion cyclotron wave absorbed at the resonances at the central cell magnetic minima. Placing the slot antenna next to the gas box produces efficient breakdown and buildup from a low density stream. With midplane fueling the neutral pressures in the plug are reduced by an order of magnitude over the case with R=4 fueling. The gas utilization efficiency is also improved by a factor of two. The central cell ion energy confinement time is not dramatically improved by midplane fueling, indicating that it is limited by charge exchange recombination with neutral hydrogen. Central cell τ_E should

approach the classical ion-ion collision time during thermal barrier operation because of lower gas fueling rates. Computer modeling of the collisional filling rate of the thermal barrier predicts that present stream ion temperatures are adequate to maintain the thermal barrier.

References:

1. Kesner, J., Post, R. S., McVey, B. D., Smith, D. K., Nuc. Fus. **22**, p. 549, (1982).

2. Post, R. S., Irby, J., Kesner, J., Mauel, M., McVey, B. D., Smith, D. K., in "Radiation in Plasmas", Ed. B. McNamara, Trieste, 1983, World Scientific, Singapore 1984.

3. Goulding, R., Golovato, S. N., and Hershkowitz, N., Bull. Am. Phys. Soc. **28**, 1202 (1983).

4. Smith, D. K., Brau, K., Goodrich, P., Irby, J., Mauel, M., McVey, B. D., Post, R. S., Sevillano, E., and Sullivan, J., Phys. Fluids **29**, p. 902, (1986).

5. Hershkowitz, N., Nelson, B. A., Johnson, J., Ferron, J. R., Persing, H., Chan, C., Golovato, S. N., Callen, J. D., and Woo, J., Phys. Rev. Lett. 55, 947 (1985).

6. Post, R. S., Gerver, M., Kesner, J., Irby, J. H., Lane, B. G., et al., Tenth Int. Conf. on Plasma Physics and Controlled Thermonuclear Fusion Research, # IAEA-CN-44/C-I-4, London, UK, Sept. 1984.

7. Breun, R., Golovato, S. N., Yujiri, L., McVey, B., Molvik, A., Smatlak, D., Post, R. S., Smith, D. K., and Hershkowitz, N., Phys. Rev. Lett. 47, 1833, (1981); Golovato, S. N., Breun, R. A., Ferron, J. R.,Goulding, R. H., Hershkowitz, N., Horne, S. F., and Yujiri, L., Phys. Fluids 28, 734 (1985).

8. Brau, K., Post, R. S., Sevillano, E., to be published in J. Vac. Sci. Tech., June 1986

9. McVey, B. D., MIT-PFC report RR-84-12, July 1984.

10. Watari, T. et al., Phys. Fluids. **21**, (1978) 2076.

11. Okamura, S., Kumazawa, R., Adati, K., Aoki, T., Fujita, H., et. al., in Plasma Physics and Controlled Nuclear Fusion Research, London, 1984 (International Atomic Energy Agency, Vienna, 1985), Vol. 2, p. 337.

12. McVey, B. D., Breun, R. A., Golovato, S. N., Molvik, A. W., Smatlak, D. L. and Yujiri, L., Bull. Am. Phys. Soc. **26**, 902 (1981).

13. Paoloni, F. J., Phys. Fluids, 18, 640 (1975).

14. Ferron, J. R., Hershkowitz, N., Breun, R. A., Golovato, S. N., and Goulding, R., Phys. Rev. Lett. 51, 1955 (1983).

15. Futch, A. H., Lodestro, C. C., "Collisional Trapping Rates for Ions in a Magnetic and Potential Well", Lawrence Livermore National Laboratory Report UCRL–87249 (1982).

Figure Captions

Figure 1. Schematics of the various gas fueling and magnetic field configurations in the Tara central cell. *a)* Single mirror cell, gas injection valves for R=1 fueling (case 1) and R=4 fueling (case 2) are shown; *b)* midplane fueling with R=2 local maximum.

Figure 2. Axial profiles of edge molecular hydrogen pressure for R=4 fueling (solid), and midplane fueling (dashed).

Figure 3. Velocity space diagram at plug midplane indicating advantages of central cell midplane fueling over fueling at R=4. ϕ_{TB} and ϕ_{cc} are the thermal barrier and central cell potentials, respectively.

Figure 4. Cutaway view of the central cell midplane gasbox.

Figure 5. Schematic of a double half turn antenna and the slot antenna.

Figure 6. Vacuum k_z spectrum of left circularly polarized electric field for m= -1.

Figure 7. Dependence of perpendicular plasma pressure at R=1.1 on position of ICRF resonance position.

Figure 8. Profile of endloss ion current during slot antenna operation.

Figure 9. *a)* Time evolution of RF power, diamagnetic signal at R=1, line-integrated density, and τ_E for the case of R=4 fueling, slot antenna only. *b)* similar plots for R=4 fueling, double half turn antenna only during steady state.

Figure 10. Data from a discharge with midplane fueling.

Figure 11. Central cell τ_E as a function of neutral pressure at the midplane.

Figure 12. Electron end loss current, deduced from Faraday cup and net current detectors, vs. central cell gas injection rate for midplane and R=4 fueling.

Figure 13. Numerical simulation of the time evolution of central cell density, ion temperature, thermal barrier potential, trapped ion density in thermal barrier, and the quantity g at the onset of thermal barrier formation for three different cases of T_i and central cell gas fueling response time (see text).

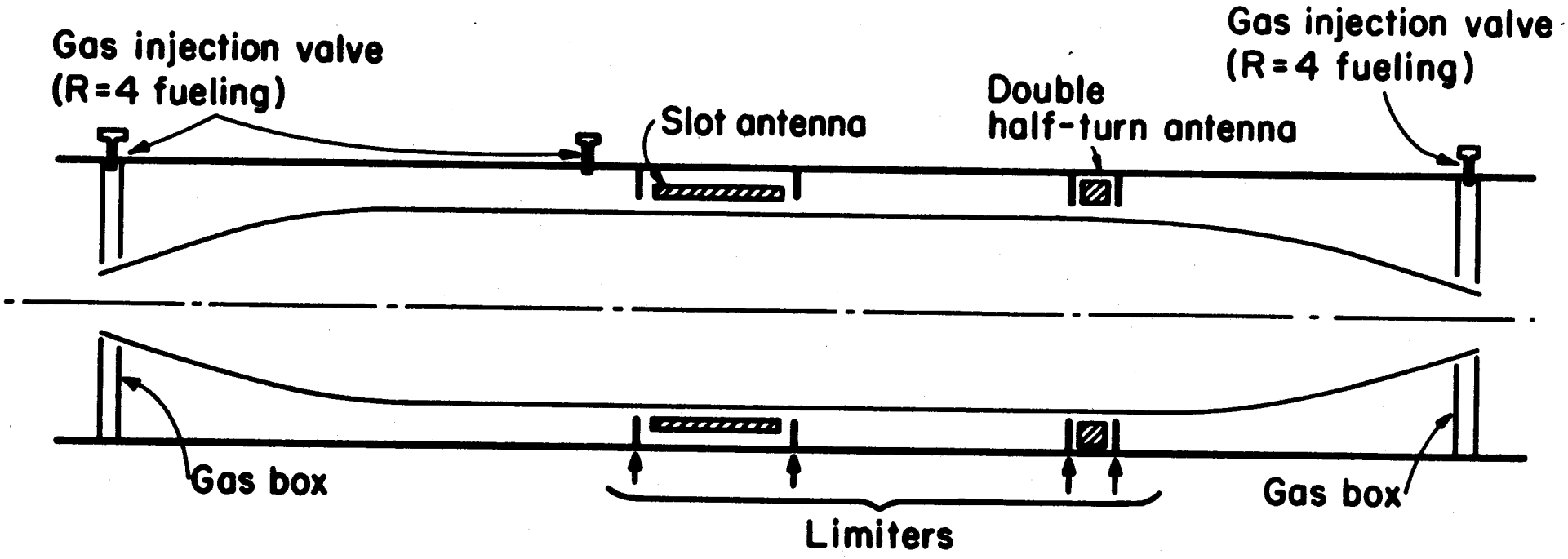
Gas injection valve
(R=4 fueling)
Slot antenna
Double
half-turn antenna
Gas injection valve
(R=4 fueling)
Gas box
Limiters
Gas box

Fig. 1a

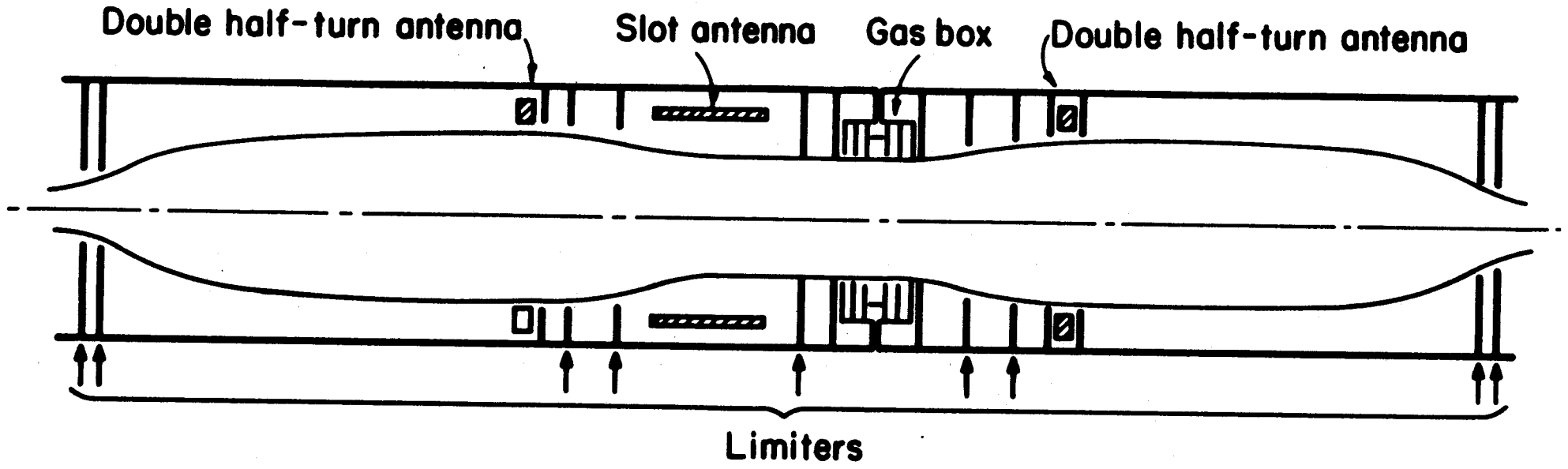
Double half-turn antenna
Slot antenna
Gas box
Double half-turn antenna
Limiters

Fig. 1b

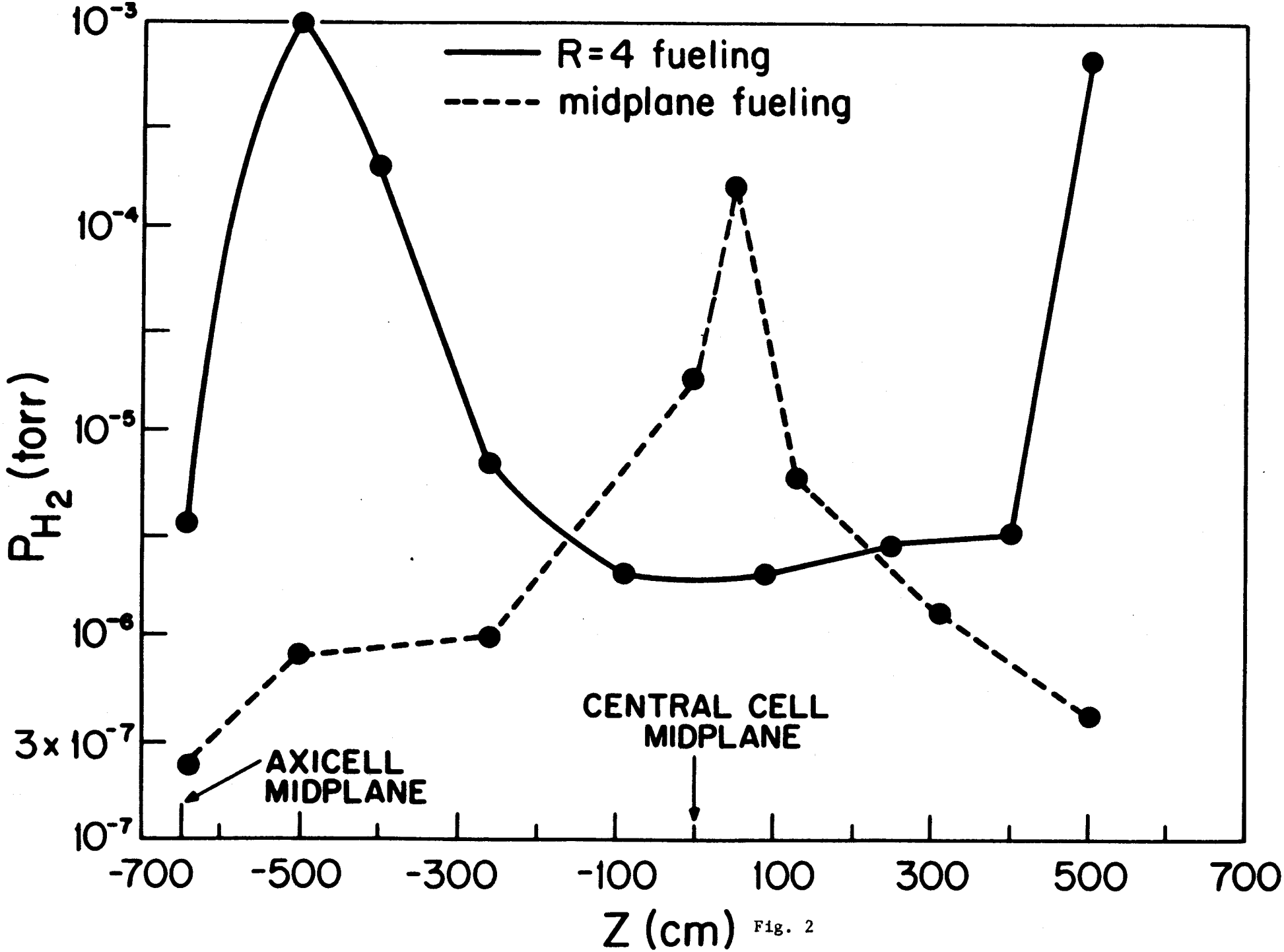
R=4 fueling
midplane fueling
10^{-3}
10^{-4}
10^{-5}
10^{-6}
3×10^{-7}
10^{-7}
P_{H_2} (torr)
AXICELL MIDPLANE
CENTRAL CELL MIDPLANE
-700
-500
-300
-100
100
300
500
700
Z (cm)

Fig. 2

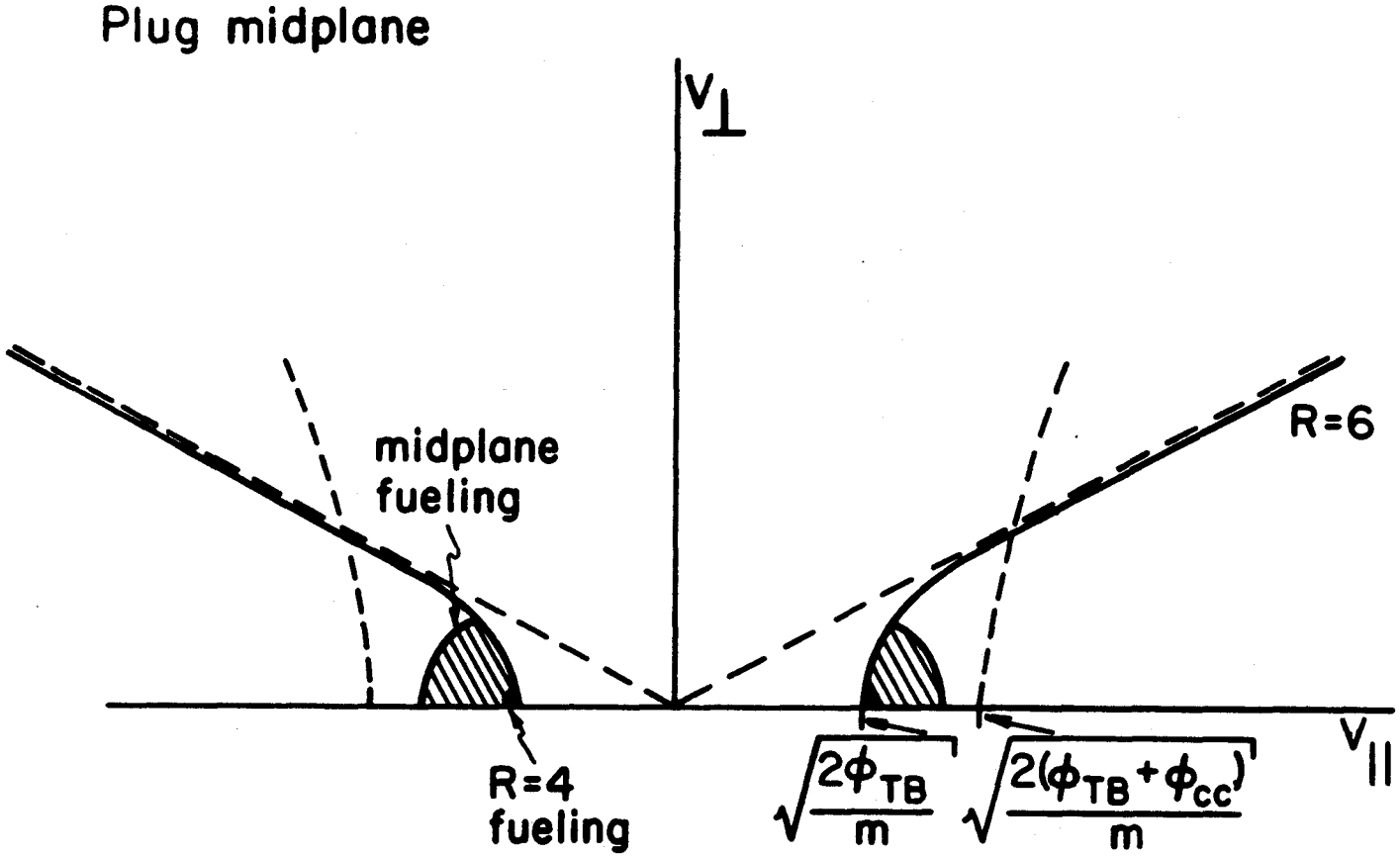
Plug midplane
$V_\perp$
midplane fueling
R=6
R=4 fueling
$\sqrt{\frac{2\phi_{TB}}{m}}$
$\sqrt{\frac{2(\phi_{TB}+\phi_{cc})}{m}}$
$V_{||}$

Fig. 3

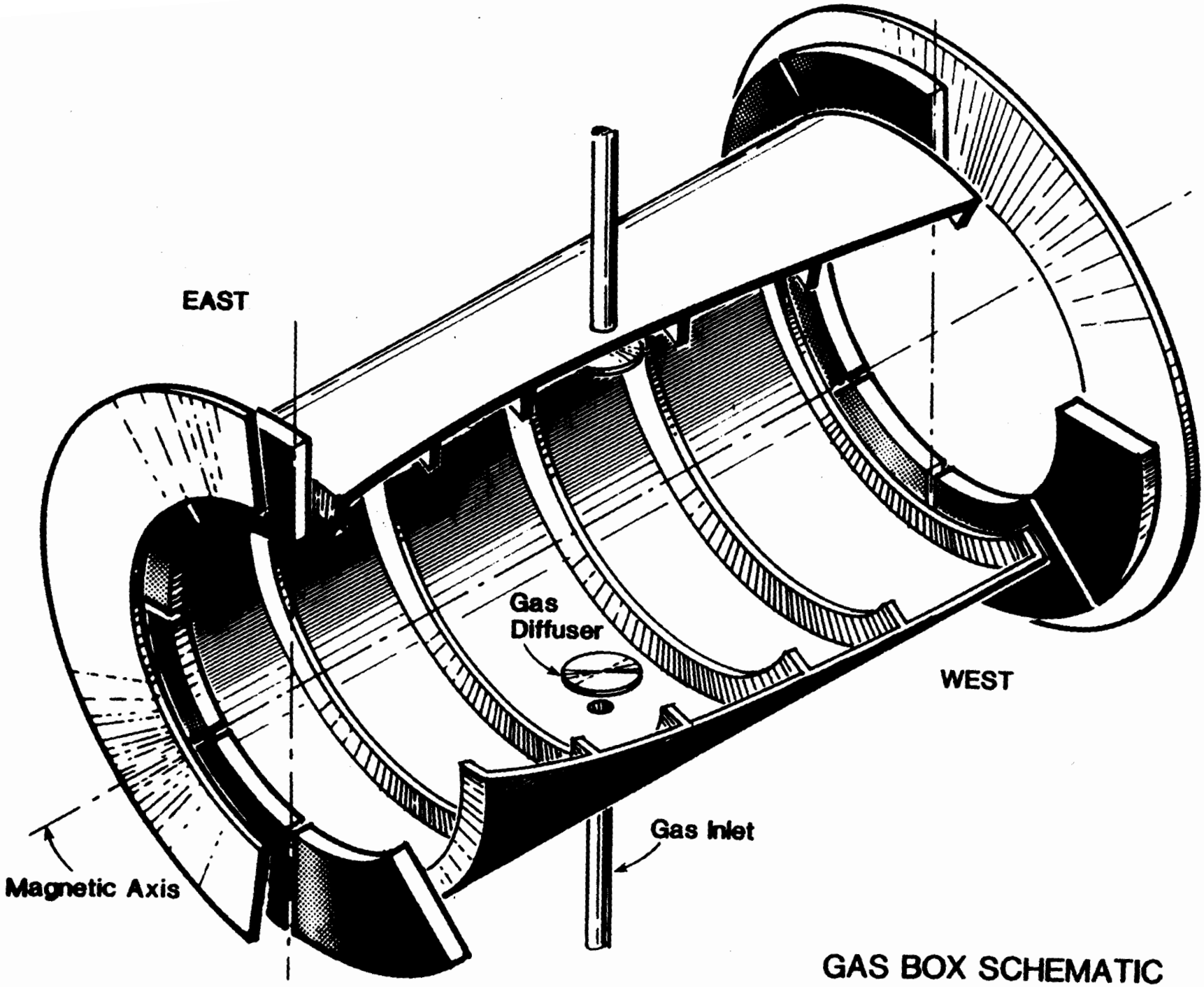
EAST
Gas
Diffuser
WEST
Gas Inlet
Magnetic Axis
GAS BOX SCHEMATIC

Fig. 4

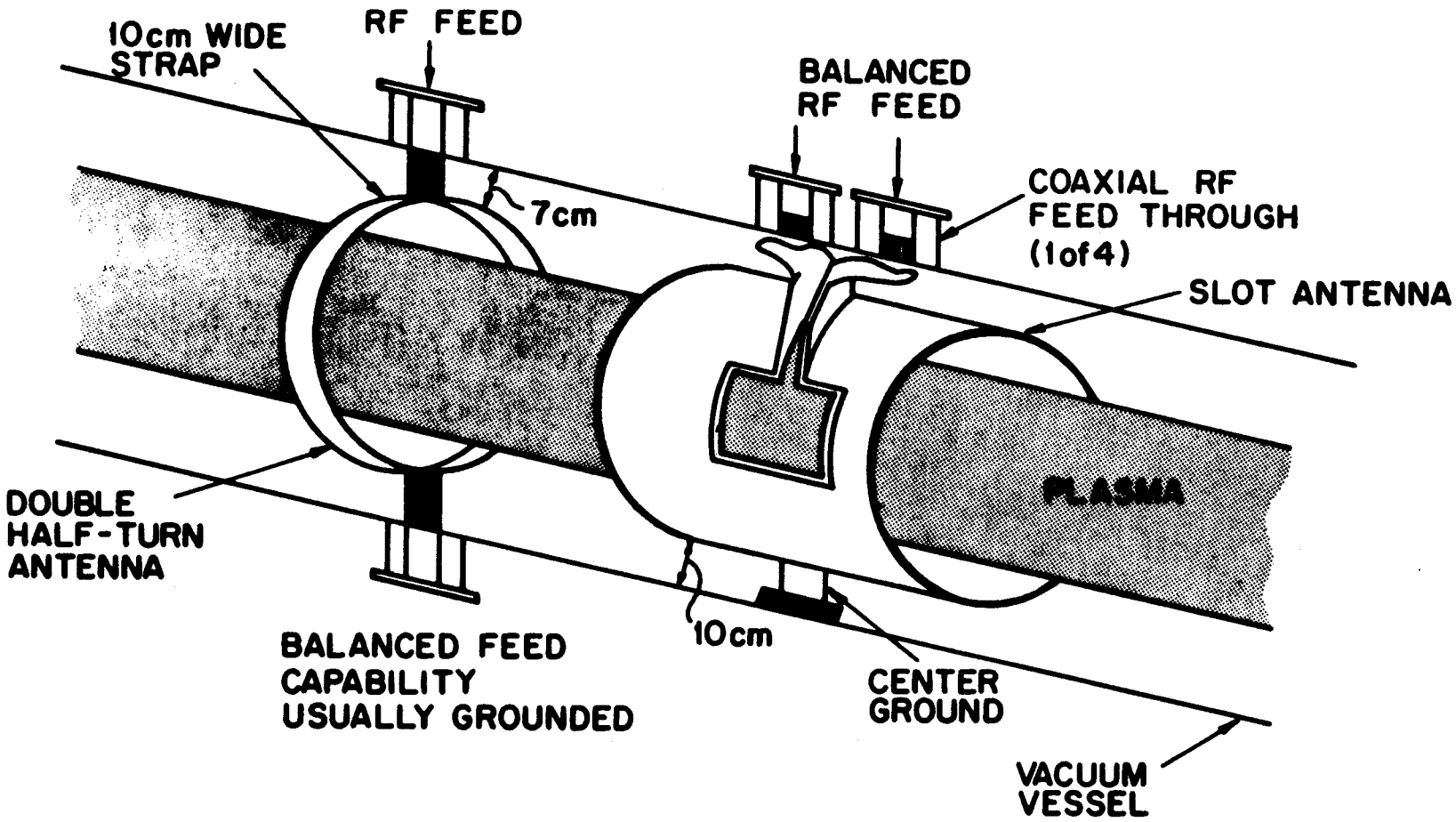

Both types of ICRF antennas shown with limiters removed

Fig. 5

Slot antenna

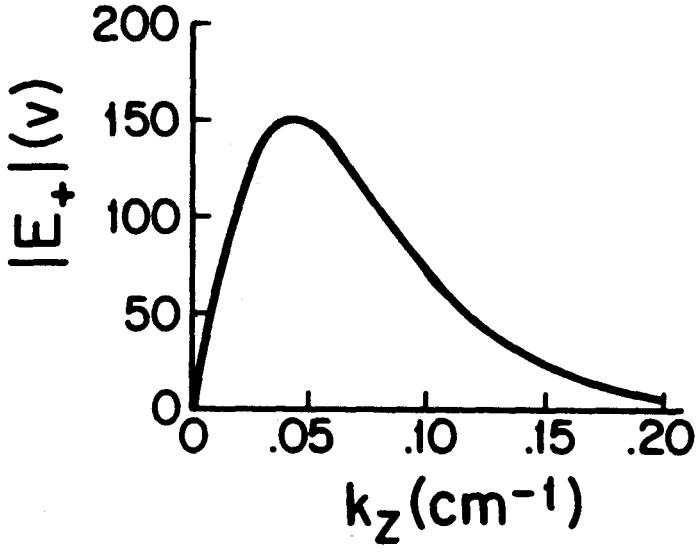

Double-half-turn antenna

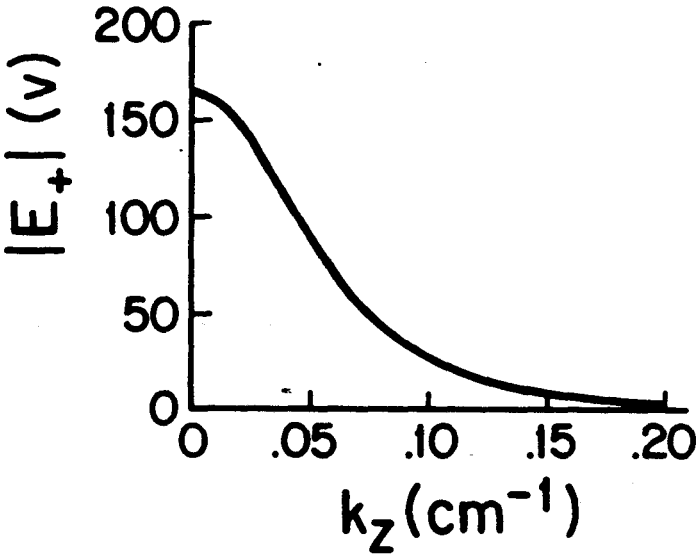

Fig. 6

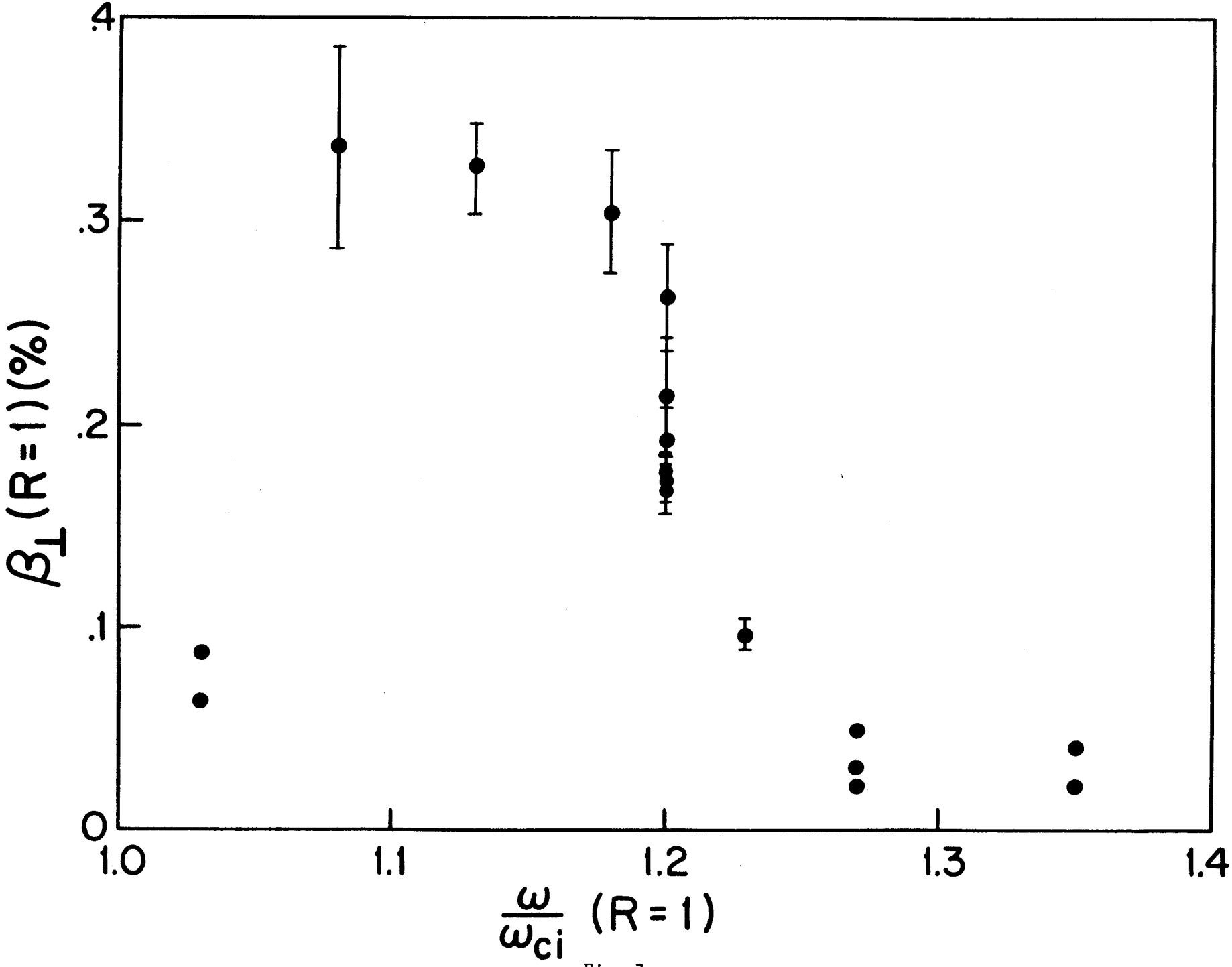

Fig. 7

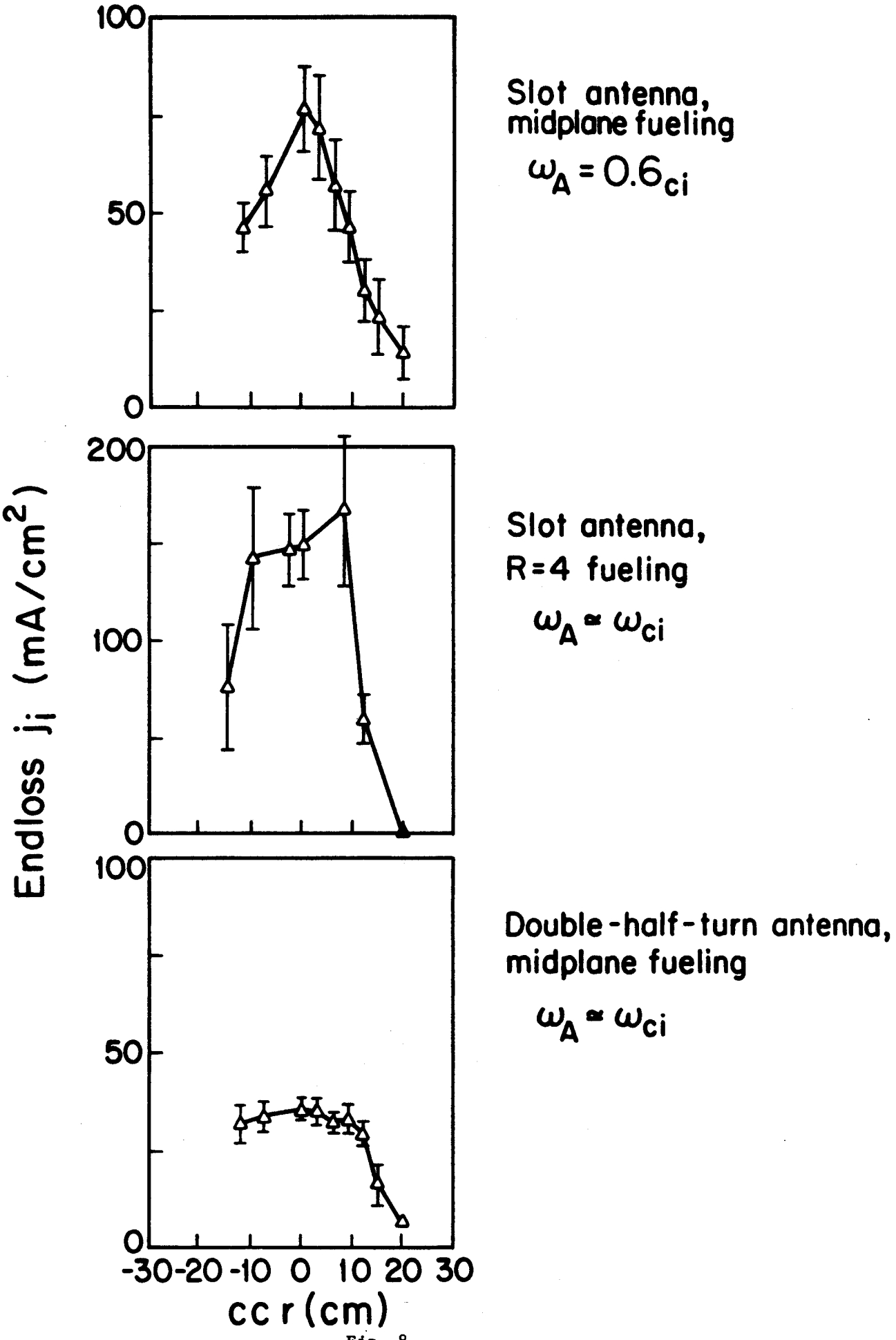
100
50
0
200
100
0
100
50
0
-30 -20 -10 0 10 20 30
cc r (cm)
Endloss j_i (mA/cm^2)
Slot antenna,
midplane fueling
$\omega_A = 0.6\omega_{ci}$
Slot antenna,
R=4 fueling
$\omega_A \approx \omega_{ci}$
Double-half-turn antenna,
midplane fueling
$\omega_A \approx \omega_{ci}$

Fig. 8

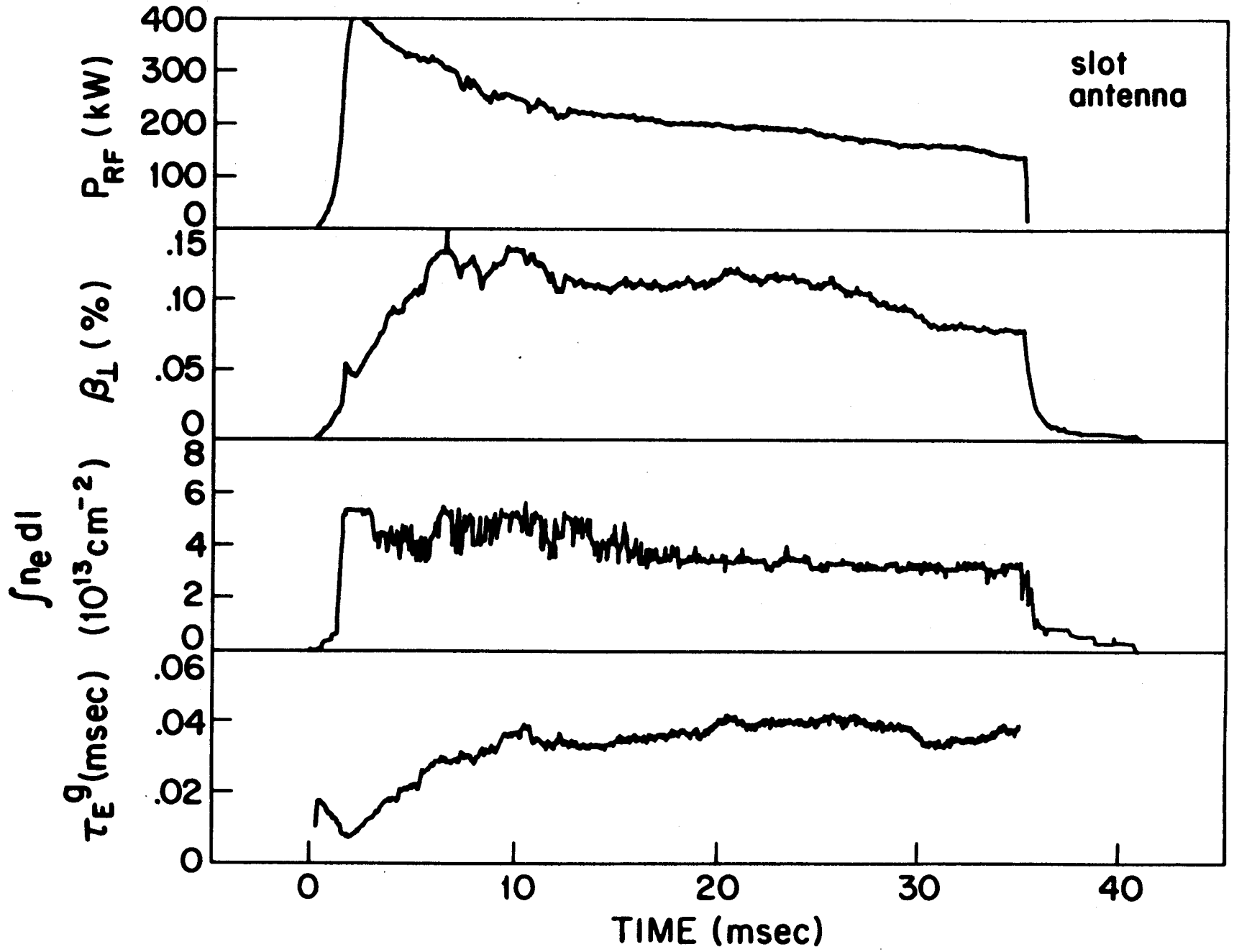
400
300
200
100
0
P_{RF} (kW)
slot
antenna
.15
.10
.05
0
$\beta_\perp$ (%)
8
6
4
2
0
$\int n_e dl$ $(10^{13} cm^{-2})$
.06
.04
.02
0
τ_E^g(msec)
0
10
20
30
40
TIME (msec)

Fig. 9a

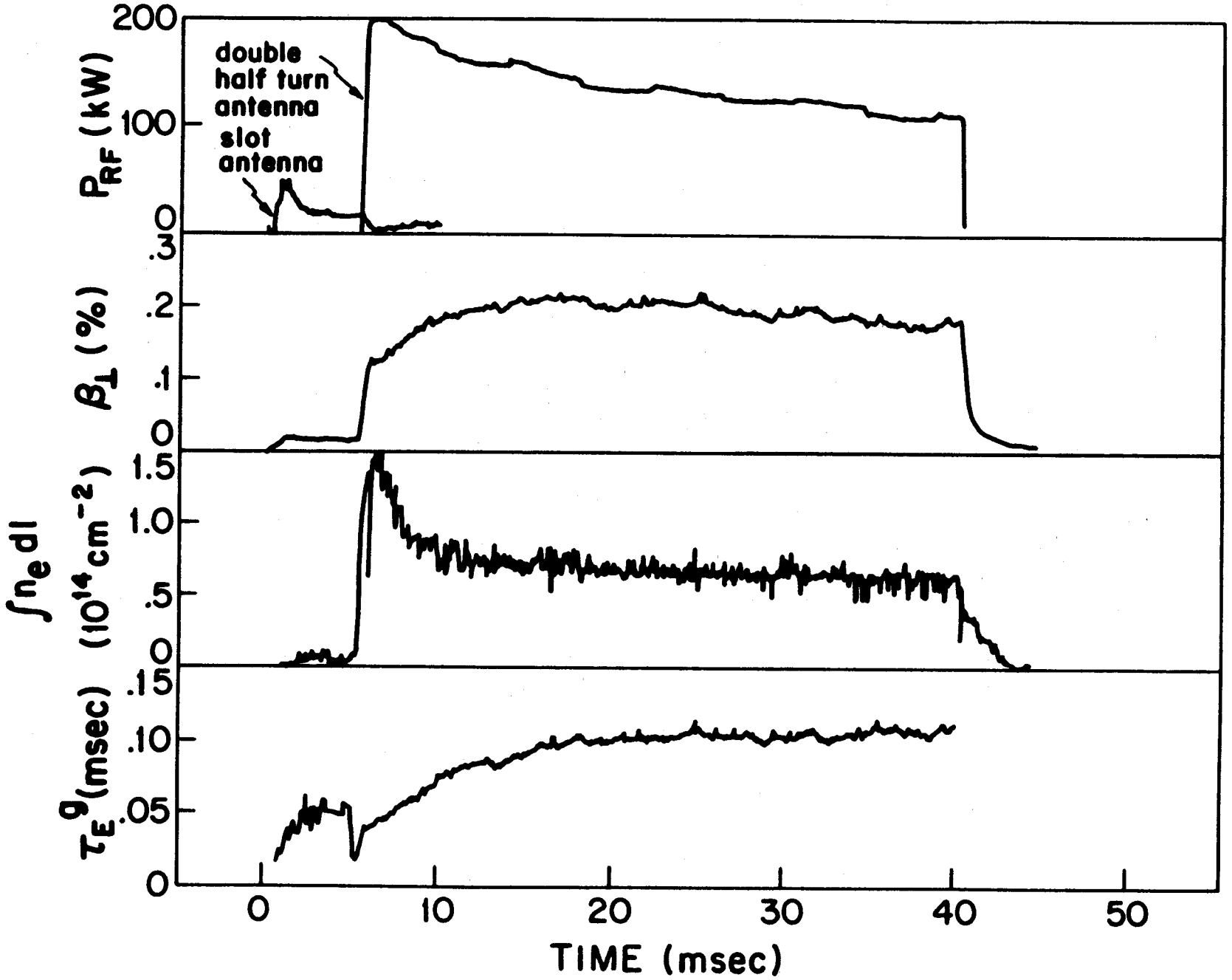
200
100
0
P_{RF} (kW)
double
half turn
antenna
slot
antenna
.3
.2
.1
0
$\beta_\perp$ (%)
1.5
1.0
.5
0
$\int n_e dl$ $(10^{14} cm^{-2})$
.15
.10
.05
0
τ_E^g (msec)
0
10
20
30
40
50
TIME (msec)

Fig. 9b

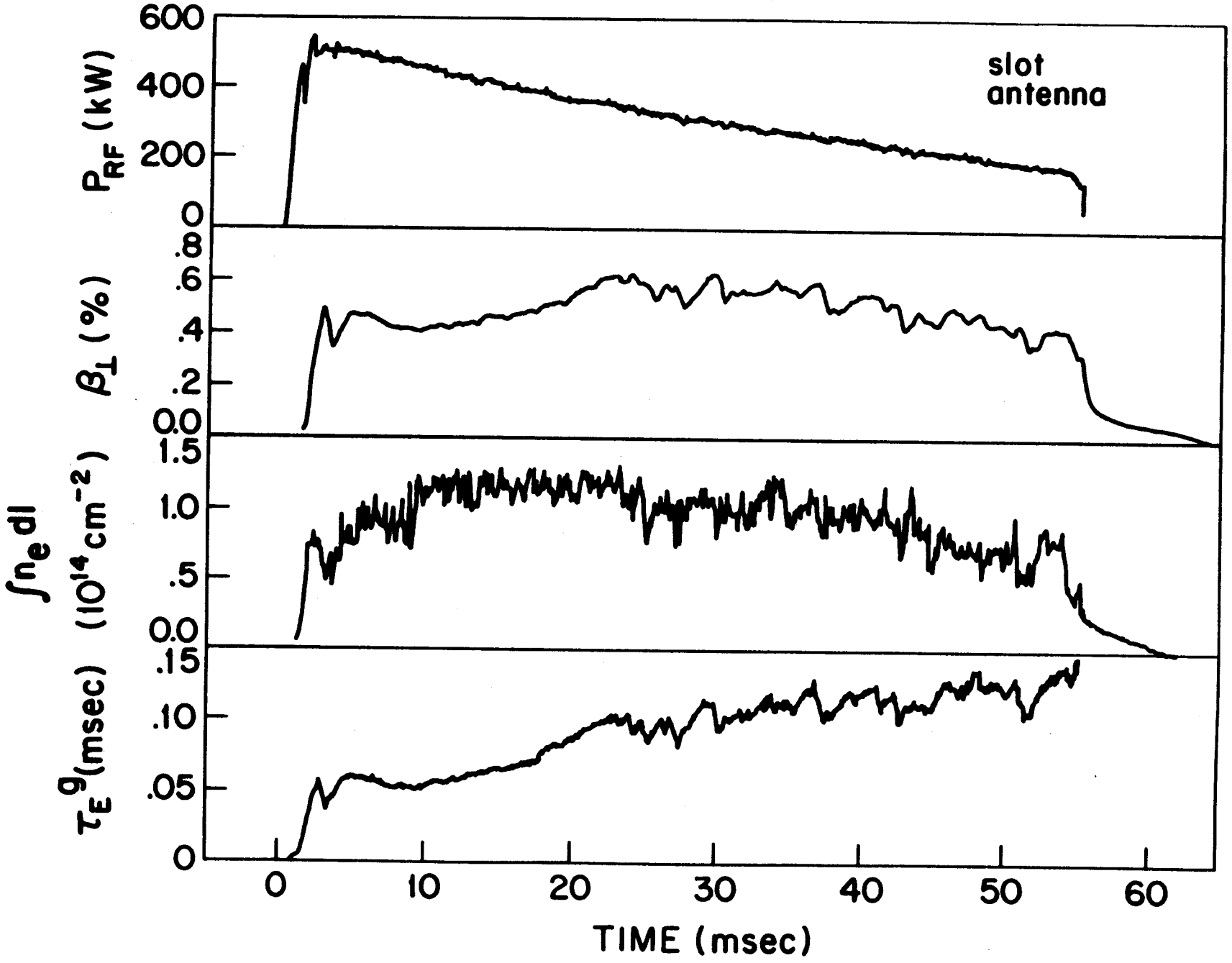
600
400
200
0
P_{RF} (kW)
slot
antenna
.8
.6
.4
.2
0.0
$\beta_\perp$ (%)
1.5
1.0
.5
0.0
$\int n_e dl$ (10^{14} cm^{-2})
.15
.10
.05
0
τ_E^g(msec)
0
10
20
30
40
50
60
TIME (msec)

Fig. 10

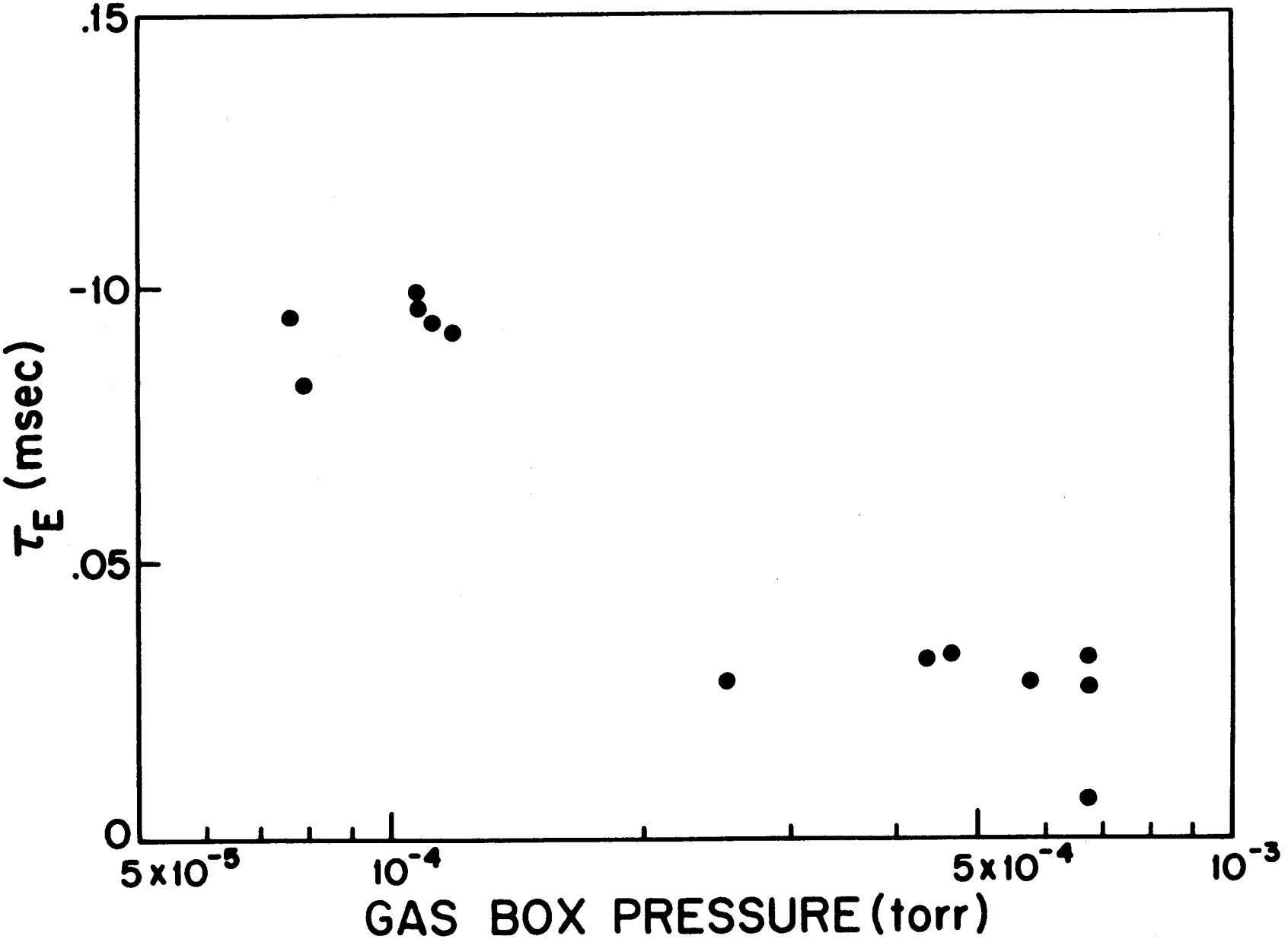
.15
.10
.05
0
τ_E (msec)
5×10^{-5}
10^{-4}
5×10^{-4}
10^{-3}
GAS BOX PRESSURE (torr)

Fig. 11

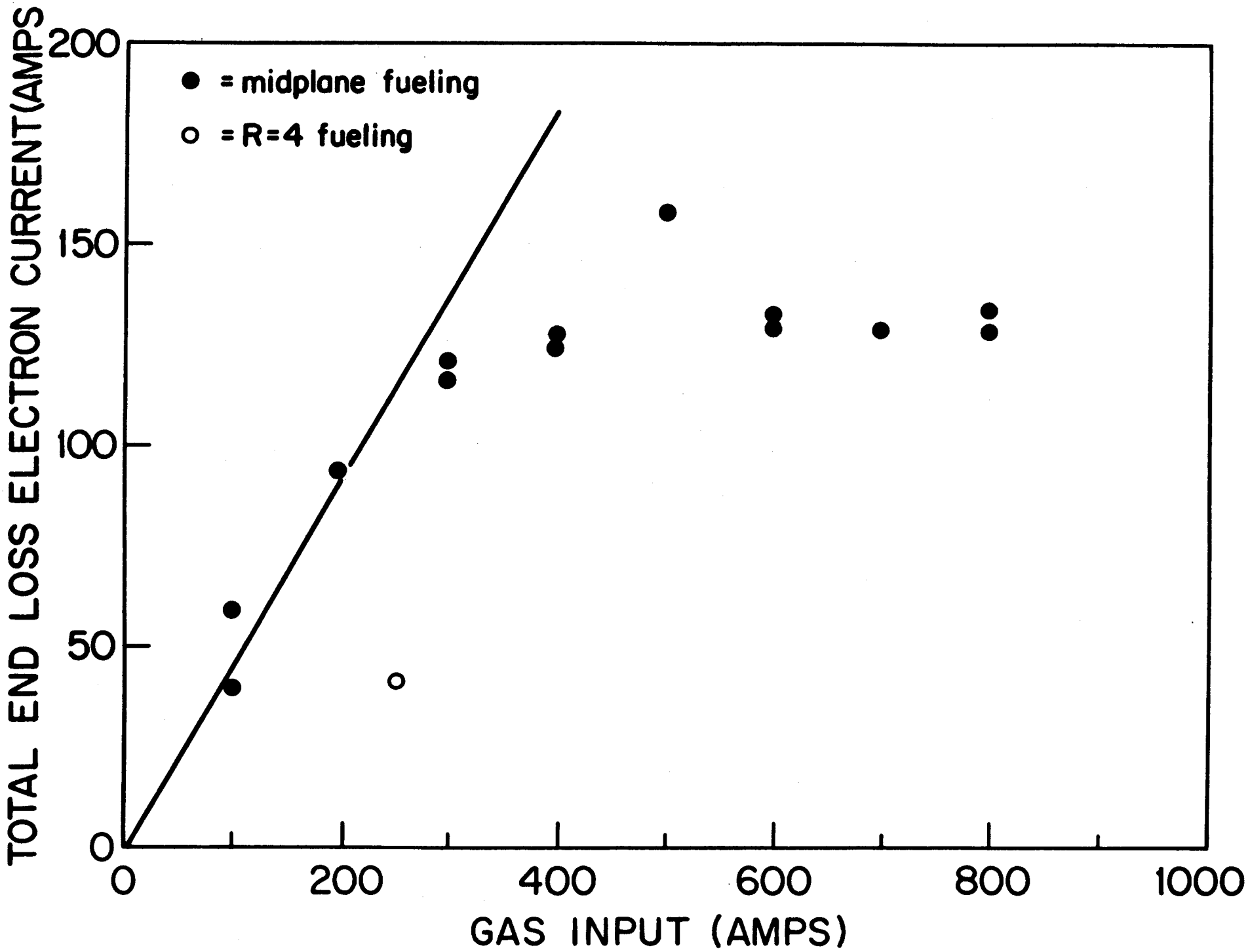
● = midplane fueling
○ = R=4 fueling
TOTAL END LOSS ELECTRON CURRENT(AMPS
200
150
100
50
0
0
200
400
600
800
1000
GAS INPUT (AMPS)

Fig. 12

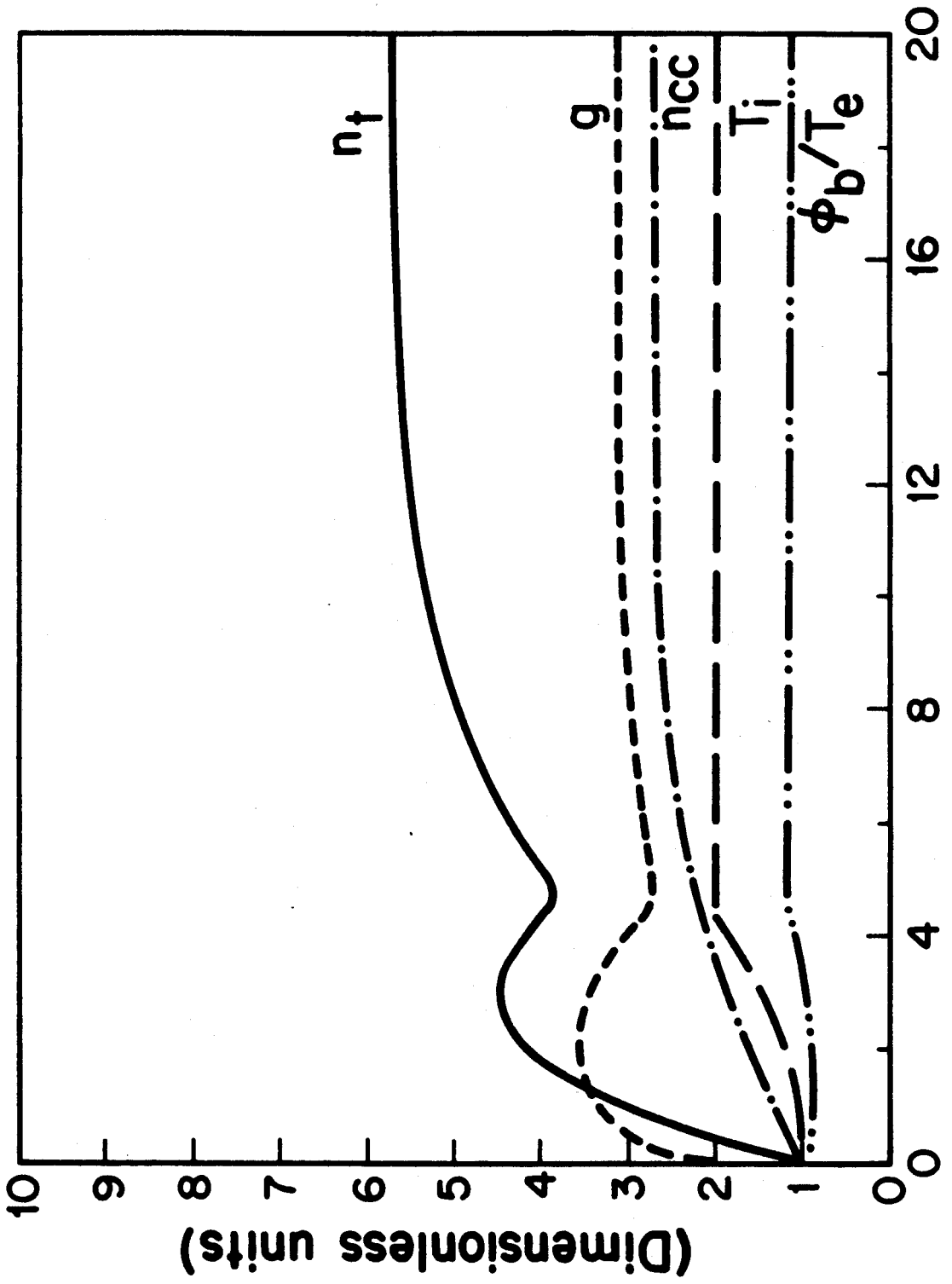
(Dimensionless units)
Time (msec)
n_t
g
ncc
T_i
ϕ_b/T_e
0
1
2
3
4
5
6
7
8
9
10
0
4
8
12
16
20

Fig. 13a

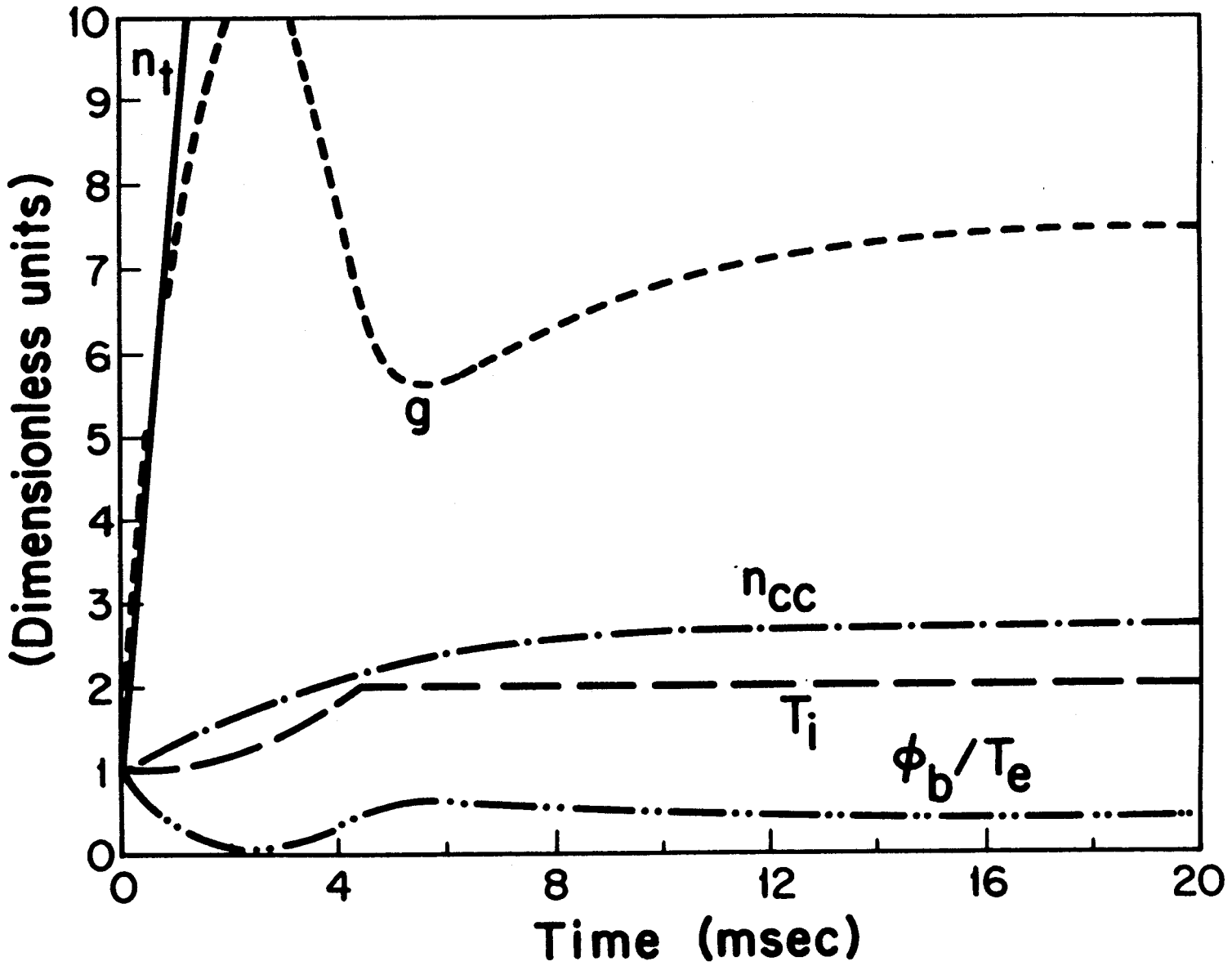
(Dimensionless units)
Time (msec)
n_t
g
n_{cc}
T_i
ϕ_b/T_e
0
1
2
3
4
5
6
7
8
9
10
0
4
8
12
16
20

Fig. 13b

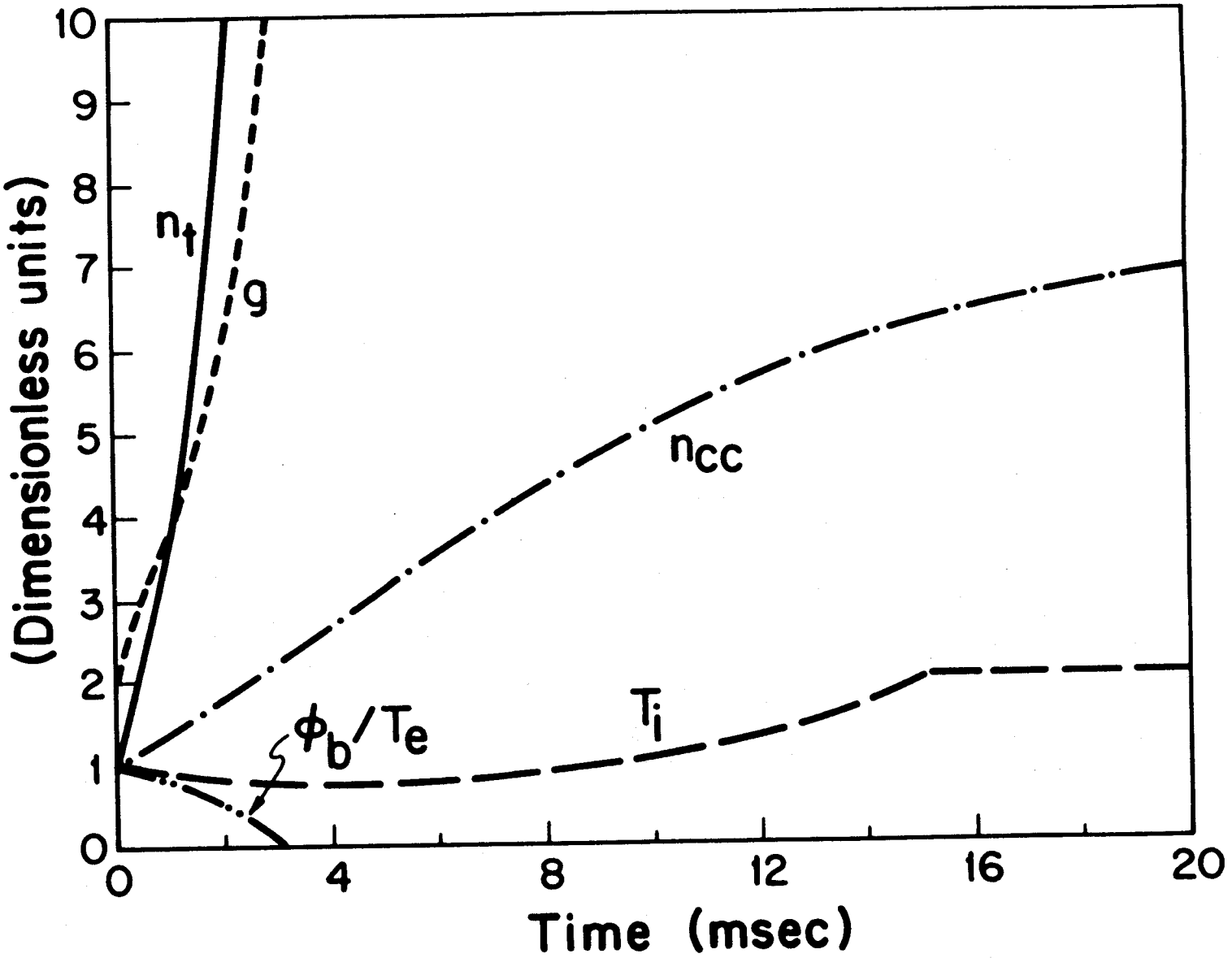
(Dimensionless units)
Time (msec)
n_t
g
n_{cc}
T_i
ϕ_b/T_e
0
1
2
3
4
5
6
7
8
9
10
0
4
8
12
16
20

Fig. 13c